JOURNAL OF MATERIALS SCIENCE **38** (2003) 3955–3963

Influence of precipitate morphology on the high-temperature deformation of Ir-Nb alloys

Y. YAMABE-MITARAI, H. HARADA
High-Temperature Materials Group, National Institute for Materials Science (NIMS), Sengen 1-2-1, Tsukuba, Ibaraki 305-0047, Japan
E-mail: mitarai.yoko@nims.go.jp

The compression strength of an Ir-15at%Nb alloy at 1473 and 2073 K was investigated. A coherent two-phase fcc $L1_2$ structure was found in the Ir-15Nb alloy. The $L1_2$ precipitate morphology depended on the heat treatment. Cuboidal $L1_2$ precipitates with a size of 100 nm and a plate-like fcc phase inside (type A) were found after heat treatment at 1773 K. The plate-like fcc phase disappeared after heat treatment at 2073 K for 24 h, and only a cuboidal $L1_2$ phase remained (type B). Coarse rectangular $L1_2$ precipitates with a length of 400 nm (type C) were found after heat treatment at 2073 K for 168 h. The influence of $L1_2$ precipitate morphology on the high-temperature strength and dislocation structure was investigated after the compression test. A bypass mechanism in which dislocations spread in the narrow fcc phase was dominant in the type A and B structures during deformation at 1473 K. In the type C structure, bypassing of precipitates was found to be dominant. At 2073 K, deformation by a shearing mechanism was dominant in the type A and B structures, while deformation by a bypassing mechanism was dominant in the type C structure. When the precipitate size was large and the fcc channel width was wide in the type B structure, a bypassing mechanism was dominant. The deformation mechanisms are discussed in terms of the precipitate morphologies.

1. Introduction

It is well known that the fcc and $L1_2$ coherent two-phase structure plays an important role in the strengthening of Ni-base superalloys, which are used under severe operation conditions in the gas turbines of generators in power stations and in jet aircraft engines [1]. In order to develop a new generation of superalloys that can be used above 1473 K, we have designed alloys with a coherent two-phase fcc and $L1_2$ structure based on Ir, which has a melting temperature of 2720 K [2]. In our previous study [3], we reported that the Ir-15 at.%Nb alloy had cuboidal $L1_2$ precipitates that were similar to those of Ni-base superalloys. However, these $L1_2$ precipitates, which had a size of 100 nm in an fcc matrix, were found to be smaller than those of the Ni-base superalloys. The precipitate morphology of the Ir-Nb alloy depended on the heat treatment [4]. As shown in Fig. 1, three classes of $L1_2$ precipitate morphologies were observed. By heat treatment at 1773 K, cuboidal coherent $L1_2$ precipitates with a size of 150 nm and a plate-like fcc phase inside (type A) were observed (Fig. 1a). The plate-like fcc phase was formed when cuboidal precipitates in the as-cast condition and with a non-equilibrium composition were changed to the equilibrium composition [5]. At 2073 K for 24 h, cuboidal coherent $L1_2$ precipitates with a size of 150 nm (type B) appeared (Fig. 1b). When the heat treatment at 2073 K was performed for 168 h, cuboidal precipitates were found to coarsen into rectangular $L1_2$ precipitates with a length of 400 nm (type C) (Fig. 1c). The rectangular shape suggests that the coherency still remained after the precipitates coarsened. In the previous study [4], the influence of precipitate morphology on strength was investigated. The strengths of type A and B structures were almost the same, and a dislocation bypass mechanism rather than a shearing mechanism was suggested because, if a shearing mechanism occurred, the type A structure would show higher strength as shown in Fig. 2 [4]. However, there has been no evidence so far of a bypass mechanism because the dislocation structure of the Ir-Nb alloys has not been clearly observed [6].

In this study, the dislocation structures of an Ir-Nb alloy with different precipitate morphology were investigated using transmission electron microscopy (TEM) after deformation at 1473 and 2073 K. The deformation mechanism of the Ir-Nb alloy was discussed in terms of the dislocation structure relating to precipitate morphology.

2. Experimental procedure

A 20 g button ingot with a nominal composition of Ir-15 at.%Nb was prepared by the arc-melting method. Cylindrical samples 3 mm in diameter and 6 mm in length were cut from the button ingot. In this study, two kinds of heat treatments, that is, at 2073 K for 24 h and at 2173 K for 4 h, were performed. Heat treatments were

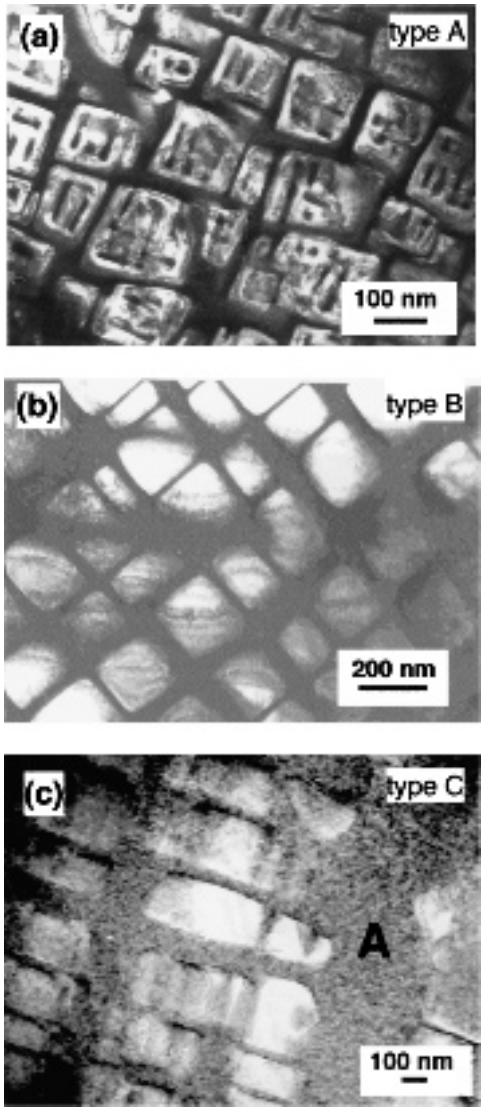

Figure 1 Dark-field images of Ir-15 at.% Nb alloys heat-treated at (a) 1773 K for 168 h, (b) 2073 K for 24 h, and (c) 2073 K for 168 h. All dark-field images were taken with a superlattice reflection ($g = 110$) from the $L1_2$ structure in the beam direction of [001].

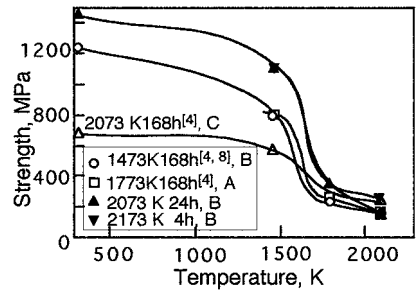

Figure 2 Temperature dependence of 0.2% flow stress.

performed in a vacuum furnace. After the heat treatment, the sample was cooled in the furnace by turning off the switch to the heater. This was done to prevent serious oxidation of the tungsten mesh heater by opening the chamber at a temperature higher than 373 K. The precipitate morphology of the sample heat-treated at 2173 K was cubic, like that of the sample heat-treated at 2073 K (Fig. 1b), although the precipitate size was about 400 nm, i.e., larger than that in the sample heat-treated at 2073 K.

Heat-treated cylindrical samples were used for the compression test in the temperature range from room temperature to 2073 K. Compression tests up to 1473 K were performed in air in TENSILON/UTM-1-50000CW testing machines. The tests above 1473 K were performed in an argon atmosphere in INSTRON 8560 testing machines. Each high-temperature test was carried out after the sample was kept at the testing temperature for 15 min. The initial compressive strain rate was 3×10^{-4}/s. The total testing time was about 20 min, including the holding time at the testing temperatures. The strain was estimated by measuring the sample length before and after the test.

The deformation structures were observed in the tested samples. In addition to the above alloys, the deformation structures of the samples heat-treated at 1773 K for 168 h and at 2073 K for 168 h [4] were also investigated. Sliced samples with a thickness of 0.2 mm were cut from the plane normal to the applied stress in the tested samples. The sliced samples were polished mechanically with SiC paper and then ion-milled. The deformation structure was then observed using a Philips CM200 transmission electron microscope (TEM).

3. Results

3.1. Microstructure

The previous study showed a microstructure change of the Ir-15Nb alloy by different heat treatments [4]. Here, we summarize the microstructure of the tested Ir-15Nb alloys. According to the binary phase diagram [7], the Ir-15Nb is in the fcc and $L1_2$ two-phase region up to 2625 K. The $L1_2$ phase is precipitated in an as-cast condition. After heat treatments at temperatures between 1473 and 2173 K, the precipitate morphology and phase composition changed to the equilibrium state [5]. Thus, we found a different morphology in the Ir-15Nb alloy by heat treatment at different temperatures, as described in the introduction. The phase compositions were not in equilibrium after heat treatment at 1473 and 1773 K, but they were in equilibrium after heat treatment above 1773 K [5]. The phase composition did not change during the short compression test.

The solubility limits of Nb in the $L1_2$ phase are about 24 at.% at heat treatment temperatures between 1473 and 2073 K. Thus, the volume fraction of the $L1_2$ phase in the Ir-15Nb alloy is about 32% by any heat treatment between 1473 and 2173 K. Because the observed area is narrow, it is difficult to measure the volume fraction of the $L1_2$ phase in TEM. In SEM, the precipitate size is too small for the volume fraction to be investigated. Therefore, we could not investigate the actual volume fraction of the $L1_2$ phase. However, the microstructure in Fig. 1 shows a similar volume fraction in the sample heat-treated at different temperatures. We compared the mechanical properties of a sample with a different $L1_2$ precipitate morphology and the same $L1_2$ volume fraction.

3.2. Compression strength behavior

The temperature dependence of the 0.2% flow stress of Ir-15Nb alloys heat-treated at different temperatures is

shown in Fig. 2. The strengths of samples with cuboidal $L1_2$ precipitates with a plate-like fcc phase (type A) by heat treatment at 1773 K for 168 h, samples with cuboidal $L1_2$ precipitates (type B) by heat treatment at 1473 K for 168 h, and samples with coarse rectangular $L1_2$ precipitates (type C) by heat treatment at 2073 K for 168 h are also plotted for reference [4, 8]. Up to 1473 K, the highest strength was shown in the type B structure with cuboidal $L1_2$ precipitates. The second highest strength was shown in the type A structure with cuboidal $L1_2$ precipitates with fcc plates. The lowest strength was found in the type C structure with a coarse rectangular $L1_2$ phase. We tested three samples of the type B structure at different heat-treatment temperatures. The strength of the type B structure obtained by heat treatment at high temperatures, such as 2073 and 2173 K, was higher than that obtained by heat treatment at 1473 K. This may be a phase-composition difference. Above 1473 K, the strength drastically dropped in all the samples, and there was no significant difference in the strengths among the alloys, which indicates that the precipitate morphology and the heat treatment temperature do not affect strengths above 1473 K.

3.3. Deformation structure

The dislocation structures of the sample tested at 1473 K were observed in TEM and are shown in Fig. 3. The compression test was stopped to observe the dislocation structure after the plastic strain reached about 3%. The actual plastic strain was estimated by measuring the sample length before and after the test. The strain values varied because the nominal strain was measured by the actuator movement during the test at high temperature and included a large degree of experimental error. Thus, the dislocation structures were observed in deformed samples with a different amount of strain.

In the type A structure, we found a dislocation contrast, which is indicated by the arrow in Fig. 3a; however, although the sample deformed about 10%, this contrast was not very clear. The dislocation contrast was very clear in the type B structure (Fig. 3b and d). In the fcc channel shown by A in Fig. 3b and d, many dislocations were observed. In the B area, straight dislocation segments aligned roughly parallel to each other are observed. This structure is similar to that observed during the incubation creep in Ni-base superalloys [9–11]. The dislocation structure was observed using methods for stereo observation in Ni-base superalloys [9]. It was then clear that these dislocations are located in the narrow fcc channels, which are aligned vertically and horizontally among the cuboidal $L1_2$ precipitates. The similarity in the microstructure suggests that dislocations are located in the fcc phase in the Ir-Nb alloy. These dislocations then spread in the narrow fcc channels.

A drastic difference was observed in the type C structure (Fig. 3c). By heat treatment at 2073 K for 168 h, cuboidal precipitates coarsened and changed to a rectangular shape (Fig. 1c). After deformation, this precipitate morphology changed from a rectangular to an ellipsoidal shape. In the A and B areas, interfacial dislocations were clearly observed by tilting the interface, which suggests that the interface is semi-coherent. A number of dislocations were observed in the fcc phase but not in the $L1_2$ phase.

Burgers vectors of dislocations were identified by contrast analysis in the sample heat-treated at 2173 K and deformed at 1473 K (Fig. 4). Dislocations were observed under the condition of a [101] zone axis. For

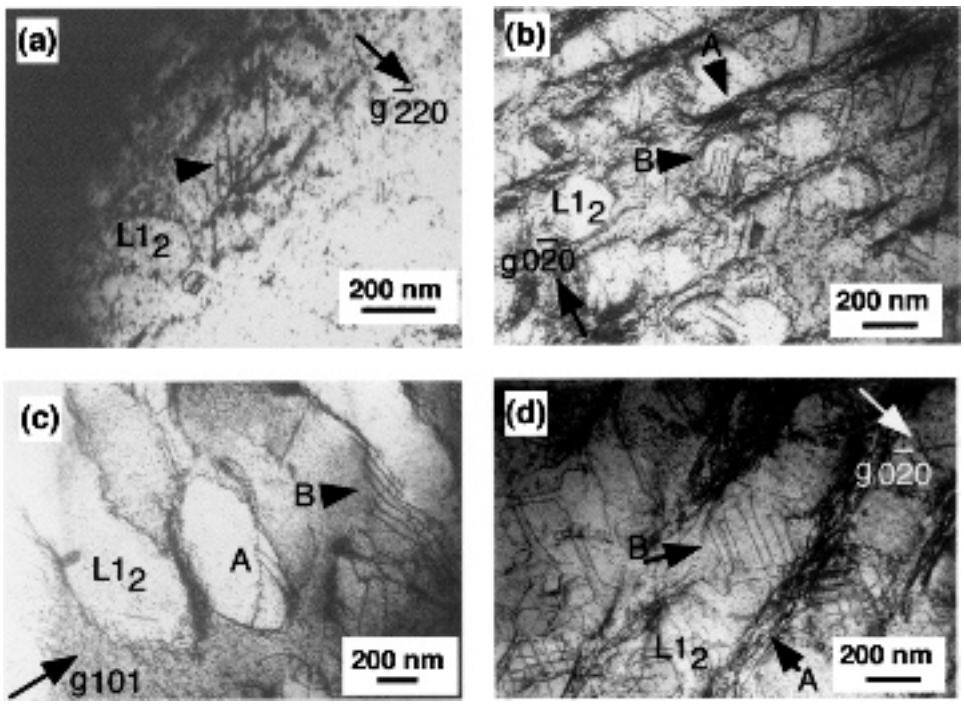

Figure 3 Dislocation structures of Ir-15 at.% Nb alloys after compression test at 1473 K after heat treatment. The heat treatment was held at (a) type A by heat treated at 1773 K for 168 h, (b) type B by heat treated at 2073 K for 24 h, (c) type C by heat treated at 2073 K for 168 h, and (d) type B by heat treated 2173 K for 4 h. The compression strain is (a) 10.61%, (b) 4.99%, (c) 5.02%, and (d) 2.46%. The zone axes are (a) [001], (b) [101], (c) [001], and (d) [101].

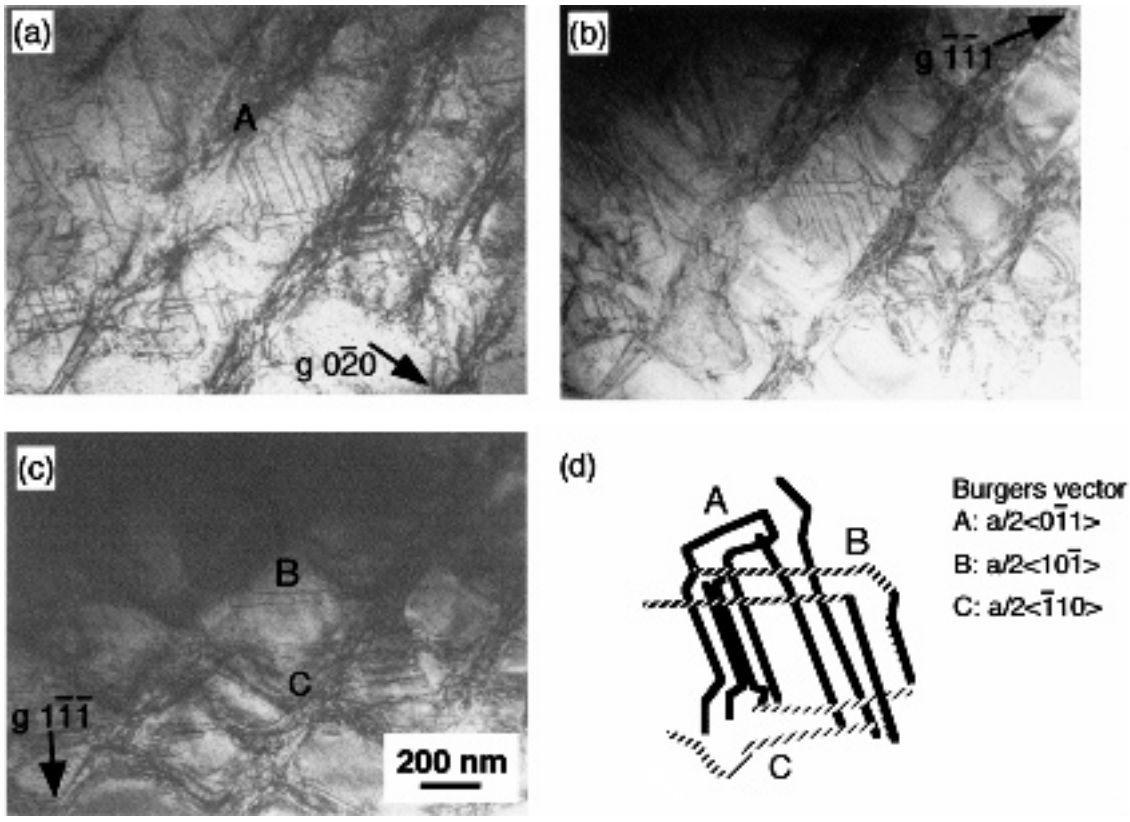

Figure 4 Contrast analysis of a deformed sample tested at 1473 K after heat treatment at 2173 K for 4 h. The zone axes are (a–c) [101]. (d) schematic diagram of Burgers vector dislocations.

example, dislocation A was visible when imaged with the reflection vector of $g = 0\bar{2}0$ and $\bar{1}\bar{1}1$ in Fig. 4a and b. However, it was not visible when imaged with the reflection vector of $g = 1\bar{1}\bar{1}$. This indicates that the Burgers vector of dislocation A is $a/2[01\bar{1}\rangle$. The Burgers vectors of other dislocations were estimated in the same way. The results of the dislocation contrast are shown in Table I. A schematic diagram of the dislocation structure is shown in Fig. 4d. In addition, the dislocation line direction of these dislocations was investigated by trace analysis. The dislocation line directions were [011] for dislocation A and [$0\bar{1}1$] for dislocations B and C. The dislocation A was an edge dislocation, and dislocations B and C were 60° mixed dislocations. The slip planes were estimated using the Burgers vector and dislocation line direction. The slip planes were (100) for dislocation A and (111) for dislocations B and C. The dislocation line direction and slip plane are also summarized in Table I.

The deformation structures after the test at 2073 K are shown in Figs 5–8. In the sample heat-treated at 1773 K (type A) and 2073 K (type B), cuboidal precipitates maintained their shape, and dislocation contrasts were not observed in either the fcc or the $L1_2$ phases (Figs 5 and 6). Instead, the fringe contrast was observed in the $L1_2$ phase, as indicated by arrows. In both samples, characterization of the fringe contour was tried by different kinds of g vectors in some zone axes. However, it was not clear if the fringe contrast showed the shearing precipitates or the tilted interface between the fcc and $L1_2$ phases. Much of the plate-like fcc phase was observed in the $L1_2$ phase before the test in the sample heat-treated at 1773 K (Fig. 1a). After the deformation, we observed only one fcc phase, as shown by A in the image (Fig. 5b).

The deformation structure of the sample heat-treated at 2073 K for 168 h (type C) is shown in Fig. 7. The precipitate morphology changed from a rectangular shape to an ellipsoidal shape. This means that the $L1_2$ precipitates coarsened and lost coherency during the test, as they did during the compression test at 1473 K. We found several dislocations and stacking faults in the fcc phase, as indicated by the arrows, which suggests that shearing occurred in the $L1_2$ phase.

After deformation of the sample heat-treated at 2173 K for 4 h (type B), we observed that the cuboidal precipitates had lost coherency and had spheroidized at the corner of the cube (Fig. 8a). In some areas, the precipitate shape was almost cubic and some shearing, albeit little, was observed in the $L1_2$ phase, but there were a few of shearing (Fig. 8b). The type B structure was obtained in two samples heated at different temperatures, 2073 K for 24 h and 2173 K for 4 h. The deformation structures of the samples

TABLE I Experimental observation of visibility (V) and invisibility (I) and Burgers vector of dislocations. The dislocation line direction and the slip plane are also summarized

	Type A	Type B	Type C
$g = 0\bar{2}0$	V	I	V
$g = \bar{1}\bar{1}1$	V	V	I
$g = 1\bar{1}\bar{1}$	I	V	V
Burgers vector	$a/2[01\bar{1}]$	$a/2[10\bar{1}]$	$a/2[1\bar{1}0]$
Dislocation line direction	011	$0\bar{1}1$	$0\bar{1}1$
Slip plane	100	111	111

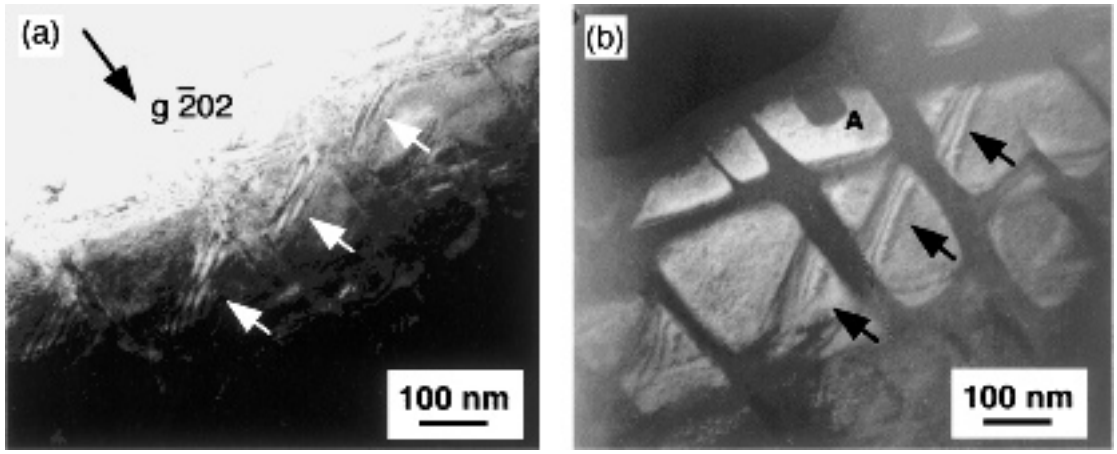

Figure 5 Dislocation structures of Ir-15 at.% Nb alloys after a compression test at 2073 K after heat treatment at 1773 K for 168 h (type A). (a) bright-field image ($g = \bar{2}02$) and (b) dark-field image taken with a superlattice reflection ($g = \bar{1}01$) from the $L1_2$ structure in the beam direction of [101]. The compression strain is 5.9%.

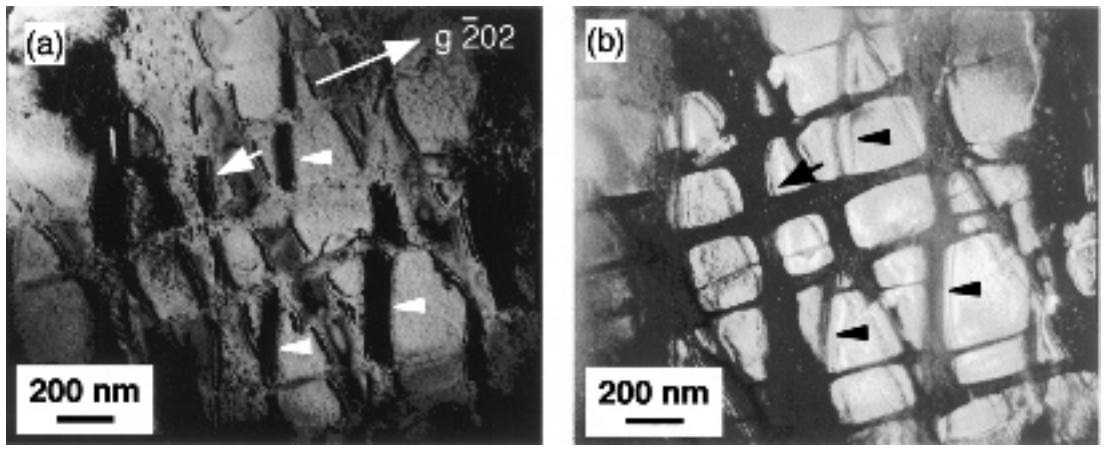

Figure 6 Dislocation structures of Ir-15 at.% Nb alloys deformed at 2073 K after heat treatment at 2073 K for 24 h (type B). The zone axis is [111]. (a) bright-field image and (b) dark-field image taken with superlattice reflection ($g = \bar{1}10$). The compression strain is not clear because of a sample crash during the test.

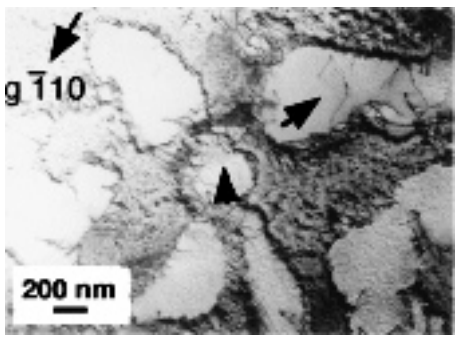

Figure 7 Dislocation structure of Ir-15 at.% Nb alloys after a compression test at 2073 K after heat treatment at 2073 K for 168 h (type C). The zone axis is [112]. The compression strain is 0.79%.

heated by the two different heat treatments were the same after deformation at 1473 K, that is, dislocations with a straight segment were observed in the fcc matrix. However, the deformation structure at 2073 K was quite different in two samples heated under different conditions. Spheroidizing was clearly observed in the sample heat-treated at 2173 K, while cuboidal precipitates remained in the sample heat-treated at 2073 K.

The deformation structure in each sample heat-treated under different conditions is summarized in Table II.

4. Discussion

4.1. Deformation mechanism at 1473 K

We observed three kinds of precipitate morphologies for three different heat treatments in the Ir-15 at.%Nb alloy. The first was a cuboidal $L1_2$ phase with an internal plate-like fcc phase (type A); the second was a cuboidal shape (type B); and the third was a rectangular shape with a length of 400 nm and a width of 200 nm (type C), as shown in Fig. 1. After the compression test at 1473 K, we did not see any evidence for shearing precipitates in any of the samples tested. This result suggests that a bypass mechanism was dominant in all three structures. However, the deformation structure was different among the tested samples heated under different conditions. Each deformation structure is discussed below.

In the type B structures, dislocations spread in the narrow fcc channels. The bypass mechanism, which shows an Orowan loop around the individual precipitates, was not observed. This suggests that the bypass

TABLE II Deformation mechanism of tested alloys at 1473 and 2073 K

Heat treatment	1773 K 168 h	2073 K 24 h	2073 K 168 h	2173 K 4 h
Structure type	A	B	C	B
Precipitate morphology	Cuboidal $L1_2$ with plate-like fcc inside	Cuboidal $L1_2$	Rectangular $L1_2$	Cuboidal $L1_2$
Precipitate size (nm)	150	150	400	300–400
Deformation structure at 1473 K	Bypass	Bypass by extending dislocation in narrow fcc	Bypass in wide fcc phase, spheroidzing	Bypass by extending dislocation in narrow fcc
Deformation structure at 2073 K	Shearing	Shearing	Bypass in wide fcc phase, spheroidzing	Bypass in wide fcc phase, spheroidzing

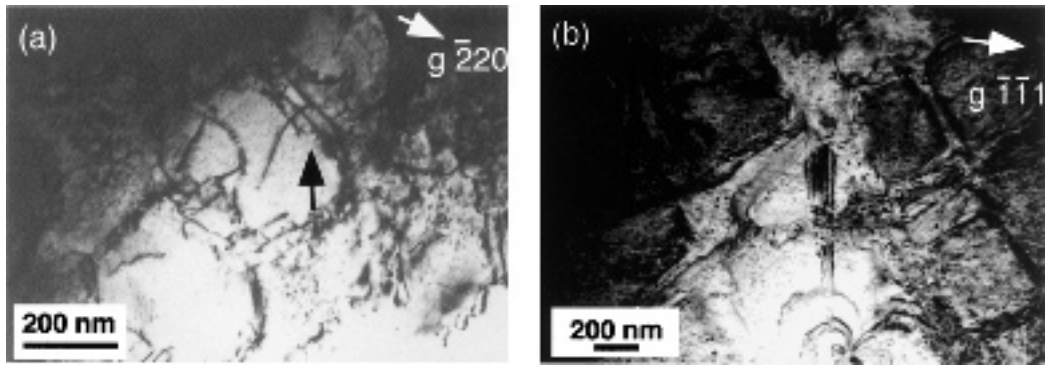

Figure 8 Dislocation structures of Ir-15 at.% Nb alloys deformed at 2073 K after heat treatment at 2173 K for 4 h (type B). The zone axes are (a) [111] and (b) [101]. The compression strain is 0.17%.

mechanism in the type B structure is different from the so-called Orowan mechanism. A similar deformation structure was observed in the Ni-base superalloys [9–11]. When cuboidal precipitates align along the ⟨100⟩ directions, only a mobile screw segment of an $a/2\langle\bar{1}10\rangle$ dislocation can bypass the $L1_2$ phase by moving through the fcc matrix, leaving segments of a mixed character on the $\langle\bar{1}10\rangle$ line direction. As shown in Fig. 9a, a dislocation with the Burgers vector of $a/2[0\bar{1}1]$ moves into the fcc phase, leaving segments of a mixed character on the $\langle\bar{1}10\rangle$ line direction. It can be said that, when relatively large precipitates align along the cube orientation, the motion of the dislocation is strictly limited through the narrow matrix channel, a structure that is generally known to prevent the formation of Orowan loops around the precipitates. In the Ir-Nb alloys, cuboidal precipitates were observed to align along the ⟨100⟩ directions. The deformation structures in Fig. 3b and d suggest that the same deformation mechanism is dominant in the type B structure in the Ir-Nb alloy. Furthermore, edge dislocations on the (100) planes (type A dislocations) can be observed in Fig. 4 and Table I. It is considered that dislocations moving on two kinds of {111} planes met and locked on the {100} planes. As shown in Fig. 9b, a dislocation with a Burgurs vector of $a/2[10\bar{1}]$ moving on a (111) plane and a dislocation with a Burgers vector of $a/2[011]$ moving on a $(\bar{1}\bar{1}1)$ plane meet and change to an edge dislocation with a Burgers vector of $a/2[110]$ on a (001) plane. The dislocation cannot move on the (001) plane because the (001) plane is not a slip plane in the fcc phase. Thus, this also prevents the motion of other dislocations in the fcc phase and increases the creep resistance.

In the type A structure, the plate-like fcc phase was not clearly observed after deformation, as shown in Fig. 3a. However, we assume that the plate-like fcc phase still existed after a short-time compression test at 1473 K because it did not disappear after a heat treatment at 1773 K for 336 h [5]. Whether or not the morphologies of the plate-like fcc phase and the $L1_2$ precipitates had changed was not clear from the results shown in Fig. 3. We did not see any evidence that the precipitates had sheared after deformation at 1473 K (Fig. 3a). We presume that dislocations are located in the narrow fcc channels (Fig. 3a), as in the type B structure. When dislocation moves only in the fcc matrix and deformation progresses by a bypass mechanism, the internal fcc phase in the cuboidal $L1_2$ precipitates in the type A structure does not affect the strength of the alloy. This is clearly shown in Fig. 2. Here, the strength of the type A structure was somewhat lower than that of the type B structure. However, the difference in the dislocation structures of type A and B structures is not clear at present.

In the deformation mode of the type C structure in the alloy heat-treated at 2073 K for 168 h, a great change in the precipitate morphology, from a rectangular to an ellipsoidal shape, was observed (Fig. 3c). Then, the fcc channel width became wider than that of the other structures. In the wide fcc matrix, dislocation is not subjected to high Orowan resistance, which is generated when a dislocation spreads in the narrow fcc channel. We assume that a dislocation can move a longer distance more easily in a wide fcc matrix than in a narrow fcc channel. Thus, the resistance of the type C structure becomes lower than that of the type A and B ones,

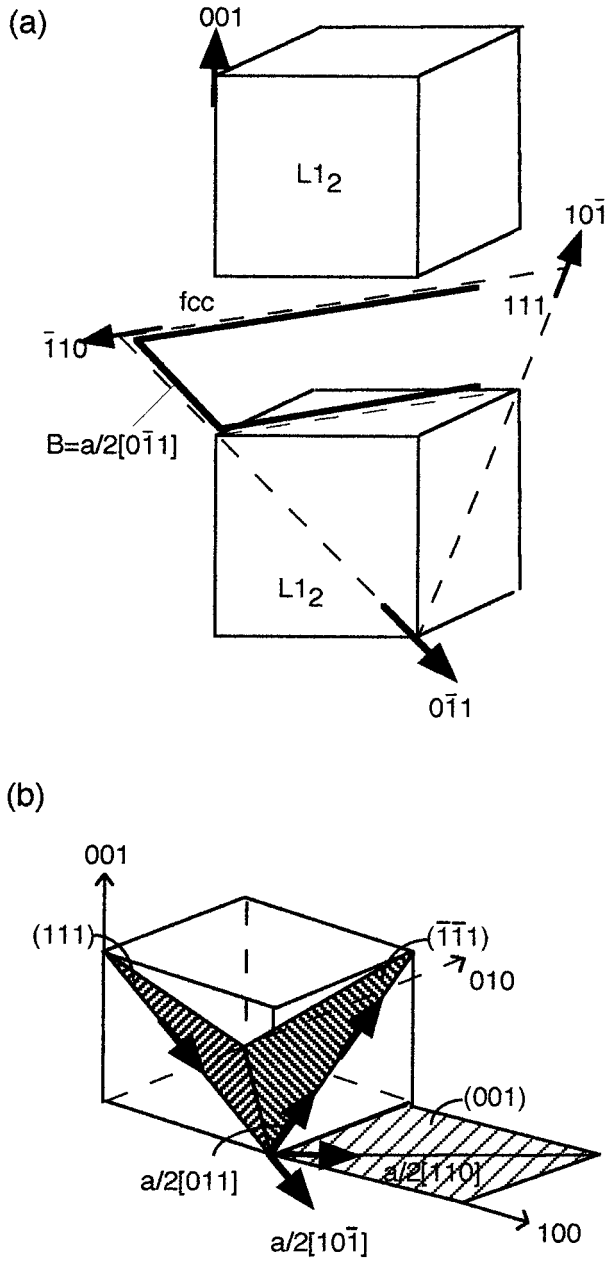

Figure 9 Schematic diagram of (a) a dislocation moving in the narrow fcc matrix between cuboidal $L1_2$ precipitates and (b) reaction between two dislocations moving on two {111} planes.

resulting in type C having the lowest strength among the tested alloys.

4.2. Deformation mechanism at 2073 K

When the testing temperature was 2073 K, there was no significant strength difference among the tested alloys. Extended dislocation in the narrow fcc channel was not observed in all of the tested samples. Instead, the shearing of precipitates was observed in the type A and B structures (Figs 5 and 6). Despite having a type B structure, the sample heated at 2173 K showed a precipitate morphology change rather than shearing (Fig. 8). A similar deformation structure, namely, a precipitate morphology change, was observed in the type C structure (Fig. 7).

Each deformation structure is discussed in detail. In the type A and type B structures heated at 2073 K, shearing of precipitates was clearly observed in the $L1_2$ precipitates (Figs 5 and 6). This suggests that the deformation resistance of the interface or the $L1_2$ phase decreased at 2073 K more than it did at 1473 K. When the resistance of shearing is small, there is no reason to bypass precipitates. Shearing then occurs easily at 2073 K. In the type A structure, few internal fcc phases were observed in the $L1_2$ precipitates in the deformed sample, while many internal fcc plates were observed in the $L1_2$ precipitates in the heat-treated sample (Fig. 1b). In the previous study, it was indicated that the internal fcc phase had almost disappeared after heat treatment at 2073 K for 20 min [5]. This suggests that the internal plate-like fcc phase had disappeared during heating before the test at 2073 K. Thus, the interface between the plate-like fcc phase and cuboidal $L1_2$ precipitates did not prevent the shearing of precipitates, and there was no more hardening effect in the type A structure than in the type B structure.

The morphology change in the precipitates was observed in the coarse microstructure formed by heat treatment at 2173 K for 4 h (type B structure) and 2073 K for 168 h (type C structure). In these two samples, the precipitate size was in the range of 300–400 nm and was found to be larger than that in the samples that showed a dominant shearing of the precipitates (150 nm). After deformation at 1473 K, the coarse rectangular precipitates also changed their shape. It is well known that two energy terms of coherent two-phase structures, i.e., elastic strain energy and interfacial energy, yield the most energetically favorable configurations to each of the precipitates [12]. When the precipitate size is larger than the critical size, the total contribution of the above two energies for the incoherent precipitate is lower than that of a coherent precipitate. Thus, large precipitates lose their coherency more easily than do fine precipitates, resulting in an accommodation of the dislocation at incoherent interfaces. Spheroidizing in the Ir-Nb alloys would seem to take place by coherency loss. After spheroidizing in the Ir-Nb alloy, the fcc matrix becomes wide in the coarse microstructure. Therefore, shearing is not necessary to move the dislocations, and the resistance to dislocation movement in the coarse microstructure decreases. Thus, the precipitation hardening effect is small.

Even when the deformation mechanism was shearing or bypassing, the strengths of the alloys tested at 2073 K was almost equivalent. This suggests that the shearing or bypassing mechanisms are not effective to strengthen the alloys at 2073 K.

4.3. Comparison with Ni-base superalloys

In Ni-base superalloys, creep tests have been performed in many studies. The simple tensile or compression test results are limited. From these limited results, dislocations were not observed extending in the fcc matrix for either the tensile or compression creep tests [13–14]. In both the tensile and compression tests, slip bands were observed in the precipitates. For example, in the tensile test at 1223 K for single-crystal Ni-base superalloy SC16 with 40% of the $L1_2$ phase volume

fraction, the dislocation structure was investigated by interrupting the tensile test [13]. During the test, dislocations appeared around the $L1_2$ particles in the initial stage; then, the dislocation density became higher, and, finally, dislocations piled up at the interface. Thus, at the end of the test, in addition to the dense dislocation pileup, slip bands were also observed. This deformation structure was similar to that obtained in our results for the sample deformed at 2073 K. The volume fraction of the Ir-15Nb alloy was about 32%, similar to that of the SC16. Furthermore, when the melting temperature of the SC16 is estimated to be about 1573K, the normalized temperature, which is estimated by the testing temperature divided by the melting temperature, is about 0.77. In our alloys, the melting temperature was 2673 K, and the normalized temperature was about 0.77. At the same normalized testing temperature and a similar $L1_2$ volume fraction, the deformation structure was found to be similar for the Ni-base superalloys and the Ir-Nb alloy. In the compression test for polycrystalline Rene95 with 55% of the $L1_2$ phase volume fraction which was slightly higher than that of the Ir-Nb alloy, stacking faults were observed in the $L1_2$ particles, and the stacking fault density increased substantially as a consequence of the reduction in the particle size [14]. These stacking faults extend across many $L1_2$ particles with a size of 0.1 μm. The testing temperature for Rene95 was 923 K, resulting in a normalized temperature of 0.58. In our results, the normalized temperature of the 1473 K testing temperature was 0.55. However, at this temperature, dislocation spreading in the narrow fcc phase was observed in the Ir-Nb alloy. The deformation structure observed in Ni-base superalloys is similar to that of the type A and type B structures heated at 2073 K (fine precipitates) and deformed at 2073 K. The lattice misfit difference, the positive and negative of the lattice misfit, and volume fraction difference are considered to be the major factors responsible for the different deformation structure; however, the reason for this difference between Ir- and Ni-based alloys is not clear.

Another difference in the comparative study of Ni-based alloys and Ir-based alloys is that single crystal was mainly used for Ni-based superalloys and a polycrystalline sample was used for the Ir-Nb alloy. In Ni-based superalloys, the selected direction of applied stress is frequently [001]. The orientation of the fcc channel is strictly vertical or horizontal to the applied stress. In addition to the Orowan resistance, misfit stresses also affect the deformation structure. In the vertical channel parallel to the applied stress, the Orowan resistance is neutralized by the misfit stress, while, in the horizontal channel normal to the applied stress, the Orowan resistance adds to the present misfit stress. The dislocations are expected to move far more easily in the horizontal matrix channels than in the vertical channels. Thus, when a deformation structure is observed in the horizontal matrix channel, long narrow loops are contained in the horizontal channels. In the vertical matrix channel, a few dislocations thread vertically through the foil. In the Ir-Nb alloys, the deformation structure depends on the orientation relationship between the applied stress and orientation of the grain boundaries. Thus, multiple slip systems are active, and cress-slip occurs. This makes it difficult for the combination of $\langle 112 \rangle$ or $\langle 110 \rangle$ dislocations to shear the precipitates.

5. Conclusions

The deformation structure of an Ir-Nb alloy with an fcc and $L1_2$ coherent two-phase structure was investigated after compression tests at 1473 and 2073 K. Three kinds of $L1_2$ precipitate morphologies were observed by different heat treatments, namely, cuboidal $L1_2$ precipitates of size 150 nm with a plate-like fcc phase inside (type A); cuboidal $L1_2$ precipitates with a size of 150 nm (type B); and coarse rectangular $L1_2$ precipitates with a size of 400 nm (type C). After the test at 1473 K, dislocations spreading in the fcc narrow channel were observed in type B. The alloy was found to be deformed by the bypass mechanism but not by the Orowan mechanism. In type A, the bypass mechanism was observed. In the type C structure, the precipitate morphology was changed to a coarse ellipsoidal shape, and dislocations were moved in the wide fcc matrix. At 2073 K, the shearing mechanism was dominant in the type A and B structures. In the type C structure, a precipitate morphology change was observed, and dislocations traveled in a wide fcc matrix. When the precipitate size was large and the fcc channel width was wide in the type B structure, bypassing dislocations were observed. However, at 2073 K, neither of the deformation structures was not effective to strengthen the alloys.

Acknowledgements

We thank Dr. T. Murakumo for his participation in helpful discussions about dislocation structure.

References

1. N. S. STOLOFF, in "Superalloys II," edited by C. T. Sims, N. S. Stoloff and W. C. Hagel (John Wiley & Sons, New York, 1987) p. 66.
2. Y. YAMABE, Y. KOIZUMI, H. MURAKAMI, Y. RO, T. MARUKO and H. HARADA, *Scripta Mater.* **35**(2) (1996) 211.
3. Y. YAMABE-MITARAI, Y. RO, T. MARUKO and H. HARADA, *Metall. Trans.* A **29A** (1998) 537.
4. Y. YAMABE-MITARAI, Y. GU, Y. RO, S. NAKAZAWA, T. MARUKO and H. HARADA, *Scripta Mater.* **41**(3) (1999) 305.
5. Y. YAMABE-MITARAI and H. HARADA, *Phil. Mag. Lett.* **3** (2002) 109.
6. Y. YAMABE-MITARAI, Y. RO, S. NAKAZAWA, T. MARUKO and H. HARADA, *Defect and Diffusion Forum* **188–190** (2001) 171.
7. "Binary Alloy Phase Diagrams," edited by T. B. Massalski (ASM, 1992) p. 1424.
8. Y. YAMABE-MITARAI, Y. GU, Y. RO, S. NAKAZAWA, T. MARUKO and H. HARADA, in Proceedings of Iridium Sympogium, "Iridium", edited by E. K. Ohriner, R. D. Lanam, P. Pannfilov and H. Harada (TMS, 2000) p. 41.
9. T. M. POLLOCK and A. S. ARGON, *Acta Metall. Mater.* **40**(1) (1992) 1.

10. S. TIAN, J. ZHANG, X. WU, H. YANG, Y. XU and Z. HU, *Met. Mater. Trans.* A **32A** (2001) 2947.
11. T. MURAKUMO, T. KOBAYASHI, S. NAKAZAWA, Y. KOIZUMI and H. HARADA, *Mater. Sci. Eng.* A (2001) accepted.
12. D. A. PORTER and K. E. EASTERLING, in "Phase Transformations in Metals and Alloys" (Chapman & Hall, London, 1992) p. 160.
13. D. MUKHERJI, H. GABRISCH, W. CHEN, H. J. FECHT and R. P. WAHI, *Acta Mater.* **45**(8) (1997) 3143.
14. S. SINHAROY, P. VIRRO-NIC and W. MILLIGAN, *Met. Mater. Trans.* A **32A** (2001) 2021.

Received 5 December 2002
and accepted 7 July 2003